

Berry monopoles and divergent quantum metric in systems with non-integer band dispersion

Jamme Omar A. Biscocho* and Kristian Hauser A. Villegas†
*National Institute of Physics,
University of the Philippines Diliman, Philippines.*

(Dated: October 21, 2024)

We investigate the quantum geometric tensor, which is comprised of the Berry curvature and quantum metric, in a generalized Dirac two-band system with non-integer dispersion, $E(\mathbf{k}) \sim k^\alpha$. Our analysis reveals that this type of dispersion introduces significant and novel effects on band geometry and topology. We calculate the Berry curvature and observe its redistribution in momentum space as α varies. Notably, despite this redistribution, the change in Chern number across topological transitions remains quantized as an integer, even for non-integer α . We illustrate the physical implications of this redistribution by computing the orbital magnetization. Furthermore, we demonstrate that the Berry curvature and quantum metric can become concentrated and even diverge in regions of momentum space where the energy band exhibits high curvature or non-analytic behavior. While it is well established that Berry curvature monopoles form at band touchings, our findings indicate that they can also emerge at sharp band corners, even in the absence of band touchings.

I. INTRODUCTION

The energy-momentum dispersion with integer exponent $E(\mathbf{k}) \sim k^n$ is well-known and ubiquitous in physics. Notable examples include the nonrelativistic free particle with $n = 2$, Dirac dispersion with $n = 1$, and flat bands with $n = 0$. In solid-state systems, where the dispersion relations are often trigonometric functions of the crystal momentum \mathbf{k} , integer-exponent dispersions arise when the energy is expanded around the band minimum. This is exemplified by the linear dispersion in graphene and the quadratic dispersion observed in semiconductors and metals. Moreover, it has been demonstrated that an N-layer ABC-stacked graphene exhibits a dispersion relation of the form $E(\mathbf{k}) \sim k^N$ [1].

A more exotic category of dispersion relations involves systems with fractional or, more generally, non-integer exponents α in the form $E(\mathbf{k}) \sim k^\alpha$. This behavior is observed in a variety of contexts, including networks with long-range transport [2], nonlocal field theories [3], optical phenomena in inhomogeneous linear media [4, 5], and fluctuations at the domain wall in superfluid-superfluid interfaces, which exhibit a dispersion relation of $E(\mathbf{k}) \propto k^{3/2}$ [6, 7]. In bilayer graphene systems, the fractional dispersion can interpolate between $\alpha = 2$ and $\alpha = 4$, with the exponent α being tunable by the displacement electric field applied perpendicular to the layers [8], a parameter easily controlled in experiments. Modifying the fractional exponent has been shown to have significant effects on various phase transitions in both bilayer and trilayer graphene systems [9].

Fractional dispersion can also be interpreted as the momentum space representation of fractional quantum

mechanics, which generalizes conventional quantum mechanics by extending derivative operators to include fractional orders [10, 11]. This framework has found diverse applications, including in entropy-area relations in black hole thermodynamics [12] and in the confinement of quarks [11, 13].

In real-space lattices, space-fractional quantum mechanics can be realized by extending the tight-binding model to incorporate infinite-range hopping, then using the Grünwald-Letnikov form of the fractional derivative [14]. This approach allows the resulting tight-binding Hamiltonian to define a Lévy crystal [15]. Such fractional media have been shown to support a variety of novel phenomena distinct from conventional quantum mechanics, including localization-delocalization transitions in one-dimensional systems [16], exotic soliton-like wave packet evolution in optical experiments [5], and the breakdown of the Mermin-Wagner-Hohenberg theorem [17]. Additionally, the effects of short- and long-range Coulomb interactions have been explored in fractional Dirac materials, demonstrating that the fractional dispersion is robust due to its nonanalytic structure [18].

In recent years, the focus of band theory in condensed matter physics has shifted from topology to geometry, effectively encapsulated by the quantum geometric tensor. The real part of this tensor, known as the quantum metric [19], measures amplitude distance, while its imaginary part, the Berry curvature, quantifies changes in phase. The Berry curvature has been extensively studied and serves as a cornerstone of modern theories of states of matter [20–23].

While the Berry curvature has received significant attention, there has been a growing interest in understanding the nature and physical implications of the quantum metric [24]. Early investigations primarily focused on superfluid weight in the superconducting phase of twisted bilayer graphene [25–27]. More recent studies have high-

* jabiscocho@up.edu.ph

† kavillegas1@up.edu.ph

lighted the crucial role of geometry in the superconducting pairing potential [28–30], as well as its effects on collective modes in superconductors [31, 32] and the enhancement of electron-phonon coupling [33].

Most existing research on band geometry has focused on conventional integer-exponent band dispersion. However, the emergence of non-integer energy band dispersions across various platforms highlights the need for a thorough investigation of their band geometry. This work fills that gap, demonstrating that fractional dispersion leads to novel and nontrivial effects on quantum band geometry.

II. FRACTIONAL DIRAC HAMILTONIAN MODEL

We start by exploring a simple model featuring fractional dispersion that exhibits a topological transition. The most minimal model capable of achieving this is a two-band system, prompting us to extend the Dirac Hamiltonian into a Bloch Hamiltonian with fractional dispersion:

$$H_\alpha(\mathbf{k}) = \text{sgn}(k_x)|k_x|^\alpha \sigma^x + \text{sgn}(k_y)|k_y|^\alpha \sigma^y + m\sigma^z. \quad (1)$$

In this expression, \mathbf{k} denotes the momentum, m represents the band gap parameter, and σ^x , σ^y , and σ^z are the Pauli matrices in the sublattice basis. The use of absolute values for the momentum components ensures that the Hamiltonian remains single-valued and exhibits parity symmetry. This model generalizes the one-band case [11] and is closely related to the framework presented in Ref. [18]. Notably, when $\alpha = 1$, the Hamiltonian reduces to the two-dimensional Dirac Hamiltonian, which undergoes a topological phase transition as the gap m varies from negative to positive. Consequently, Eq. (1) represents the fractional generalization of the two-dimensional Dirac Hamiltonian.

Additionally, we observe that the fractional Dirac equation can be derived in real space through a generalized factorization of the Schrödinger equation, akin to how Dirac derived his equation from the Klein-Gordon equation. In this framework, special values of $\alpha = 2/N$ (for positive integers N) characterize an internal $SU(N)$ structure of the particle [11].

While our model is sufficiently complex to exhibit nontrivial phases, it is also simple enough to allow analytical calculations of the Berry connection and curvature. The eigenstates are

$$\psi_\pm(\mathbf{k}, \alpha) = \frac{1}{\sqrt{2d(\mathbf{k}, \alpha)[d(\mathbf{k}, \alpha) \pm m]}} \times \begin{pmatrix} m \pm d(\mathbf{k}, \alpha) \\ d_1(\mathbf{k}, \alpha) + id_2(\mathbf{k}, \alpha) \end{pmatrix} \quad (2)$$

which correspond to the eigenvalues

$$E_\pm(\mathbf{k}, \alpha) = \pm \sqrt{d_1(\mathbf{k}, \alpha)^2 + d_2(\mathbf{k}, \alpha)^2 + m^2} \quad (3)$$

$$\equiv \pm d(\mathbf{k}, \alpha), \quad (4)$$

where $d_1(\mathbf{k}, \alpha) = \text{sgn}(k_x)|k_x|^\alpha$ and $d_2(\mathbf{k}, \alpha) = \text{sgn}(k_y)|k_y|^\alpha$.

In Fig. 1 (a)-(d), we present the two bands for various values of α . For $\alpha = 0$, we observe two flat bands, while $\alpha = 1$ corresponds to a massive Dirac band (with $m \neq 0$). For all positive values of α , a zero value of m leads to a closing of the gap between the upper and lower bands. Specifically, for these values of α , the band gap is given by $\Delta E = 2|m|$.

In contrast, the case of $\alpha = 0$ behaves differently; there is no gap closing when $m = 0$ because the band gap is given by $\Delta E = 2\sqrt{2 + m^2}$. Later, when we analyze the change in Chern number, we will show that this case does not exhibit a topological phase transition as m varies across $m = 0$, in contrast to the scenarios where $\alpha > 0$.

We further observed that non-integer values of α break the continuous rotational symmetry of the band structure in momentum space around $\mathbf{k} = 0$, reducing it from $SO(2)$ to C_4 symmetry. For $0 < \alpha < 1$, the energy bands exhibit non-analytic behavior along the k_x and k_y axes as shown on Fig. 1 (b). In contrast, for $\alpha > 1$, shown in Fig. 1 (d) the energy band surfaces take on a flat, square profile in the vicinity of the origin, $\mathbf{k} = 0$. These energy band surfaces become more rectangular with four sharp corners for larger α .

III. BERRY CURVATURE

Next, we examine the Berry curvature of the bands. Since the Berry curvature of the valence band is simply the negative of that for the conduction band, it suffices to present the results for the conduction band only. In Fig. 1 (e)-(h), we display the Berry curvature. The flat band ($\alpha = 0$, Fig. 1 (e)) shows a uniform Berry curvature of zero, while the Dirac band ($\alpha = 1$, Fig. 1 (g)) exhibits the typical isotropic Berry curvature distribution. For $0 < \alpha < 1$ (Fig. 1 (f)), the Berry curvature is highly concentrated along the k_x and k_y axes, where the corresponding energy bands exhibit nonanalytic behavior. In the case of $\alpha > 1$, the Berry curvature forms four "petals" located in each of the four quadrants of the $k_x - k_y$ plane. As α increases, the energy bands take on rectangular shapes, and Berry monopoles emerge at the four sharp corners.

In all scenarios, the Berry curvature is concentrated where the band curvature $\nabla^2 E(\mathbf{k})$ is large. While it is commonly understood that Berry curvature tends to localize at band touching points, our analysis reveals a broader observation: Berry curvature tends to be concentrated at locations of significant and nonanalytic band curvature. This pronounced curvature can occur even in the absence of band touching, as evidenced along the axes for $0 < \alpha < 1$ and at the quadrants in the \mathbf{k} plane for $\alpha > 1$.

We now investigate the integral of the Berry curvature

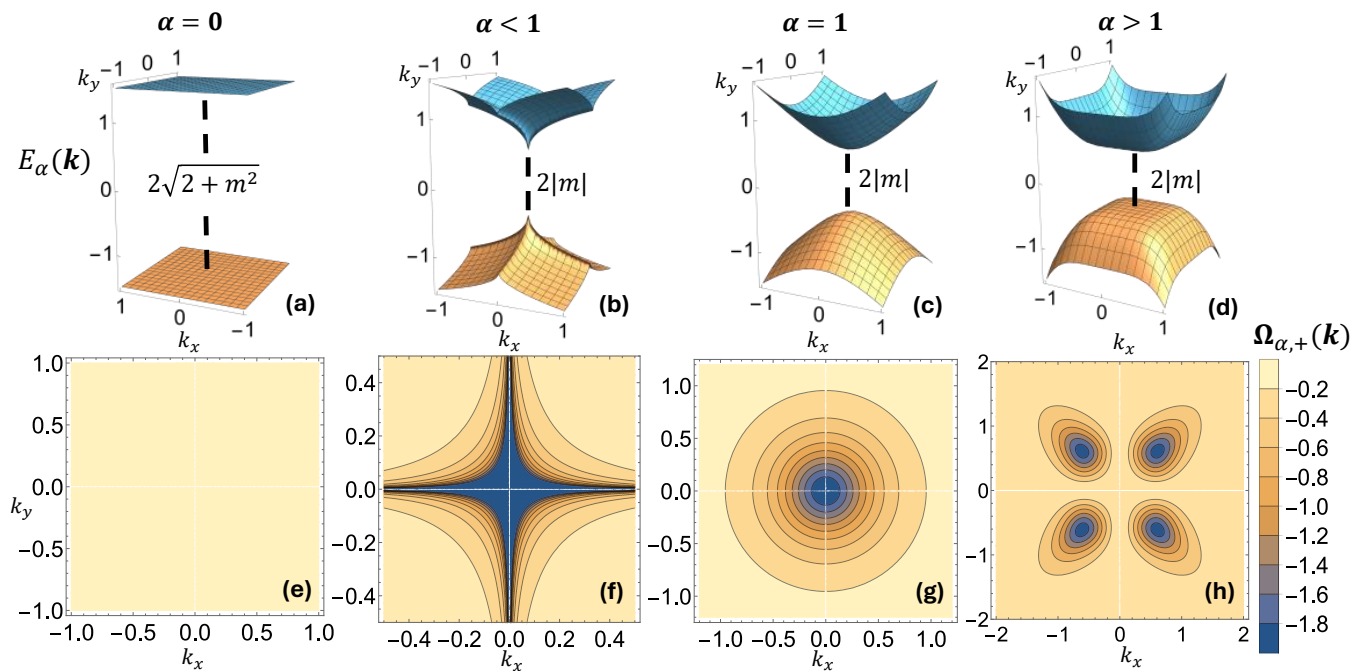


FIG. 1. The plots depict the energy bands (a)-(d) and the Berry curvature (e)-(h) of the conduction band for various values of α with $m = 0.5$. In panels (b) and (f), we set $\alpha = 0.3$, while in panels (d) and (h), $\alpha = 2.5$. The expressions next to the dashed lines in panels (a)-(d) indicate the magnitude of the band gap.

over momentum space:

$$C = \frac{1}{2\pi} \int_{-\infty}^{\infty} \int_{-\infty}^{\infty} dk_x dk_y \Omega_{xy}(\mathbf{k}, m, \alpha). \quad (5)$$

This integration is performed over the entire \mathbf{k} -space since our model, as described by Eq. (1), is based on the continuum Dirac Hamiltonian. It is important to note that the Dirac Hamiltonian does not possess a proper Brillouin zone; instead, its energy bands extend indefinitely [34, 35]. As a result, the quantity defined in Eq. (5) is not quantized to integer values and technically does not represent a Chern number, which is only defined for compact \mathbf{k} spaces. However, the *change* in C across a possible topological transition, as the gap varies from $m = -1$ to $m = 1$, yields an integral value [34, 35] and can be interpreted as a change in the Chern number across this transition.

We compute this change as follows:

$$\Delta C = C|_{m=+1} - C|_{m=-1}. \quad (6)$$

As shown in Fig. 2 (a), we find that ΔC is quantized to the integer value -1 , even for non-integer values of $\alpha > 0.5$. In the interval $0 < \alpha < 0.5$, however, the Berry curvature spreads along the axes, requiring a larger momentum region for integration to accurately capture the change in the Chern number. This explains the observed deviation from $\Delta C = -1$ in the figure.

In the special case where $\alpha = 0$, the situation is different. As seen in Fig. 1 (e), the Berry curvature is uniformly zero across momentum space, remaining so even

as m varies from negative to positive. This results in $\Delta C = 0$, indicating that there is no topological transition when m is varied across zero for $\alpha = 0$. This conclusion is consistent with our previous discussion, where we noted the absence of band gap closing at $m = 0$ for $\alpha = 0$.

IV. ORBITAL MAGNETIZATION

To explore the possible experimental consequences of the Berry curvature distribution in systems with non-integer energy-momentum dispersion, we calculate the orbital magnetization [22, 36, 37]. In magic-angle graphene, for example, the orbital magnetism can be imaged using a scanning superconducting quantum interference device [38]. Here we have two contributions: the local orbital magnetization

$$\mathbf{M}_{orb}^{loc} = \frac{1}{(2\pi)^3} \mathcal{I}m \sum_n \int_{E_{n\mathbf{k}} \leq \mu} d^2k \langle \partial_{\mathbf{k}} \psi_{n,\mathbf{k}} | \times H_{\mathbf{k}} | \partial_{\mathbf{k}} \psi_{n,\mathbf{k}} \rangle \quad (7)$$

and the itinerant contribution

$$\mathbf{M}_{orb}^{it} = \frac{1}{(2\pi)^3} \mathcal{I}m \sum_n \int_{E_{n\mathbf{k}} \leq \mu} d^2k \langle \partial_{\mathbf{k}} \psi_{n,\mathbf{k}} | \times (E_{n,\mathbf{k}} - 2\mu) | \partial_{\mathbf{k}} \psi_{n,\mathbf{k}} \rangle, \quad (8)$$

where μ is the chemical potential.

Here, we consider the conduction band only. The total orbital magnetization M_{orb} has an explicit proportional-

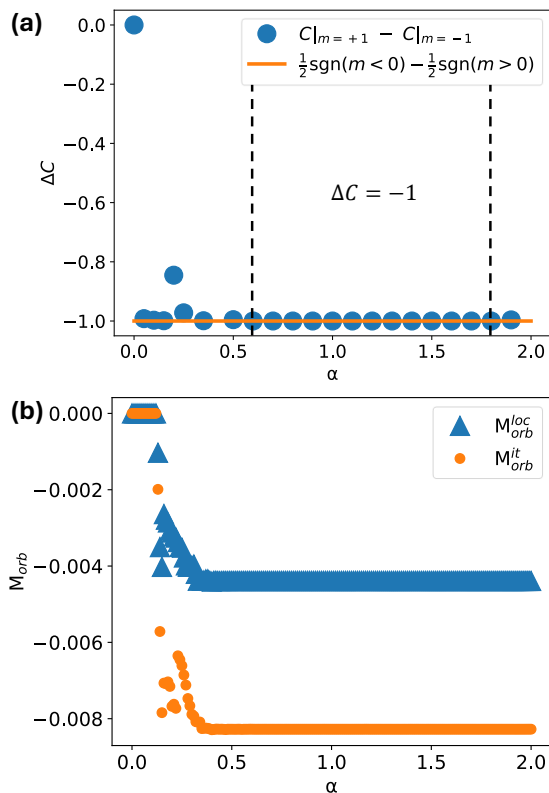


FIG. 2. (a) Difference in C between $m = +1$ and $m = -1$, over $\alpha \in [0, 2]$. The solid orange line is the change in the Hall conductance across $+m$ to $-m$ for a Dirac fermion in the continuum. The region within the dashed lines denotes the range of α where ΔC was evaluated to be exactly -1 . (b) Plot of the local M_{orb}^{loc} and the itinerant contributions M_{orb}^{it} to the orbital magnetization for $\mu = 1$ over $\alpha \in [0, 2]$.

ity with the integral of the Berry curvature [39]

$$\mathbf{M}_{orb} = \frac{2}{(2\pi)^2} \int_{E_{\mathbf{k}} \leq \mu} d^2k \mu \Omega(\mathbf{k}). \quad (9)$$

We show our results on Fig. 2 (b). The orbital magnetization is constant in the range $\alpha \gtrsim 0.4$. This is because while the Berry curvature is redistributed inside the momentum region $E_{\mathbf{k}} \leq \mu$ as α is varied, it does not spread outside the integration region, rendering the integral constant. We found that this constant magnetization persists for larger α , but the numerical integration must be refined as the Berry curvature becomes highly localized into four monopoles. For $0 < \alpha < 0.4$, some of the Berry curvature leaks out of the integration region as shown in Fig. 1 (f), resulting in decreased orbital magnetization magnitude. At exactly $\alpha = 0$, the orbital magnetization contributions are zero since the Berry curvature vanishes identically in the entire momentum space as previously shown in Fig. 1 (e). This behavior holds even if m is varied from negative to positive, which is consistent with our result above that there is no topological transition for $\alpha = 0$.

V. QUANTUM METRIC

We now calculate the quantum metric

$$g_{ij}(\mathbf{k}, \alpha)_{\pm} = \langle \partial_i \psi_{\pm}(\mathbf{k}, \alpha) | \partial_j \psi_{\pm}(\mathbf{k}, \alpha) \rangle - A_i(\mathbf{k}, \alpha)_{\pm} A_j(\mathbf{k}, \alpha)_{\pm}, \quad (10)$$

where $\mathbf{A}(\mathbf{k}, \alpha)_{\pm}$ is the Berry connection and the \pm index labels the upper and lower band cases. This gives us the information about the overlap of the states in \mathbf{k} space. We show on Fig. 3 the determinant and trace of the quantum metric. It is sufficient to show the metric invariants for the upper band since the lower band have identical quantum metric components. For the flat band, $\alpha = 0$, the quantum metric is zero everywhere in the momentum space as shown in Fig. 3 (a) and (e). This tells us that all the states have zero overlap and are therefore well-localized. We found similar results when m is varied across $m = 0$, which is consistent with previous results that there is no band gap closing, Fig. 1 (a), and that there is no change in the Chern number, Fig. 2 (b). Hence, for the flat band case, our model describes a trivial insulator for all values of m .

For non-integer dispersions, $0 < \alpha < 1$, the quantum metric components are divergent along the momentum space axes as shown on Fig. 3 (b) and (f). This mirrors the non-analytic regions of the band dispersion and the Berry curvature, Figs. 1 (b) and (f), respectively. The states along the axes in this case are therefore highly overlapping.

For the massive Dirac band case shown in Figs. 3 (c) and (g), $\alpha = 1$, we found the typical isotropic and smooth peak at the center of the momentum space. For $\alpha > 1$, Figs. 3 (d) and (h), we found four smooth peaks, one for each quadrant in the momentum space. These peaks are found at the same locations of the four “petals” of the Berry curvature in Fig. 1 (h), which, in turn, as discussed above, are located at the corners of the rectangular-like surface of the energy band. In all cases, we found that the peaks in the quantum metric occurs at the locations where the energy band curvature is high, implying that the states in these regions are highly overlapping.

VI. CONCLUSIONS

To summarize, our calculations reveal that a non-integer dispersion introduces significant and novel effects on band geometry and topology. Specifically, we observe that the Berry curvature and quantum metric become concentrated and can even diverge in momentum space regions where the energy band exhibits high curvature or non-analytic behavior, such as the kinks along the axes for $0 < \alpha < 1$ and the corners for $\alpha > 1$.

The divergence of the quantum metric along the axes for $0 < \alpha < 1$ is particularly noteworthy. In previously studied Hermitian systems, the quantum metric has primarily been considered in terms of corrections, enhancing

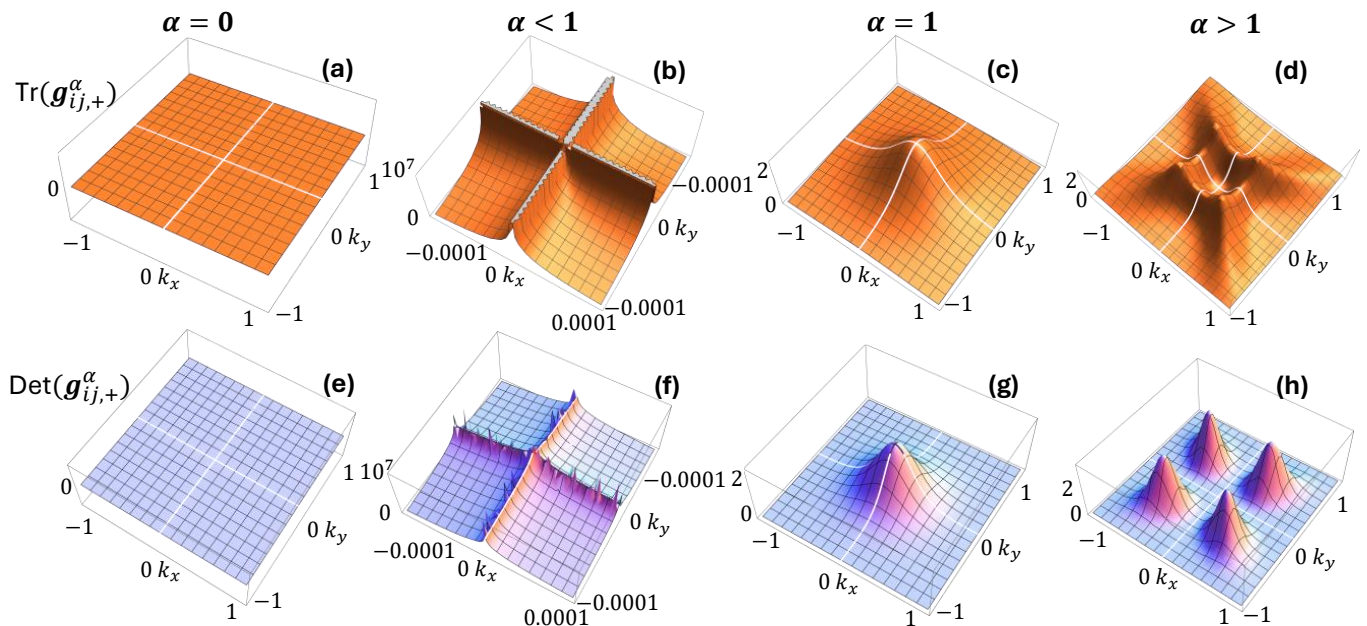


FIG. 3. The plots illustrate the trace (a)-(d) and the determinant (e)-(h) of the quantum metric for the conduction band across different values of α , with the band gap parameter set to $m = 0.5$. In panels (b) and (f), we used $\alpha = 0.3$, while in panels (d) and (h), $\alpha = 2.5$.

various physical properties. For instance, recent work on the impact of isolated singularities in the quantum metric demonstrated an increase in the BKT temperature in flat-band superconductors [40]. While divergent quantum metrics have been predicted and observed in non-Hermitian systems, where they significantly influence wave packet dynamics [41, 42], our findings indicate that such divergences can also occur in Hermitian systems.

Moreover, while it is well understood that Berry

monopoles form at band touchings, our results show that they can also arise at sharp band corners, even without band touchings. These sharp corners are specifically a consequence of non-integer dispersion. The distinct patterns of peaks and divergences in the quantum metric across different values of α suggest that state overlaps are markedly influenced by non-integer dispersion. This insight opens avenues for engineering desirable physical properties related to wave dynamics and transport in future research.

-
- [1] F. Zhang, B. Sahu, H. Min, and A. H. MacDonald, Band structure of *abc*-stacked graphene trilayers, *Phys. Rev. B* **82**, 035409 (2010).
- [2] A. P. Riascos and J. L. Mateos, Fractional quantum mechanics on networks: Long-range dynamics and quantum transport, *Phys. Rev. E* **92**, 052814 (2015).
- [3] K. G. Atman and H. Şirin, Quantization of nonlocal fields via fractional calculus, *Physica Scripta* **97**, 065203 (2022).
- [4] A. Iomin, Fractional Schrödinger equation in gravitational optics, *Modern Physics Letters A* **36**, 2140003 (2021).
- [5] Z. Zakeri, M. Solaimani, L. Lavaei, and S. A. A. Terohid, The exotic behavior of the wave evolution in Lévy crystals within a fractional medium, *Scientific Reports* **13**, 20747 (2023).
- [6] H. Watanabe and H. Murayama, Nambu-Goldstone bosons with fractional-power dispersion relations, *Phys. Rev. D* **89**, 101701 (2014).
- [7] H. Watanabe, Counting rules of Nambu-Goldstone modes, *Annual Review of Condensed Matter Physics* **11**, 169 (2020).
- [8] Z. Dong, M. Davydova, O. Ogunnaike, and L. Levitov, Isospin- and momentum-polarized orders in bilayer graphene, *Phys. Rev. B* **107**, 075108 (2023).
- [9] Z. M. Raines, L. I. Glazman, and A. V. Chubukov, Unconventional discontinuous transitions in isospin systems, *Phys. Rev. Lett.* **133**, 146501 (2024).
- [10] N. Laskin, *Fractional quantum mechanics* (World Scientific Co. Pte. Ltd., Singapore, 2018).
- [11] R. Herrmann, *Fractional Calculus: An Introduction for Physicists* (World Scientific Co. Pte. Ltd., Singapore, 2014).
- [12] S. Jalalzadeh, F. R. da Silva, and P. V. Moniz, Prospecting black hole thermodynamics with fractional quantum mechanics, *Eur. Phys. J. C* **81**, 632 (2021).
- [13] M. Abu-Shady, R. R. Luz, G. X. A. Petronilo, A. E. Santana, and R. G. G. Amorim, On the fractional quark-antiquark confinement and symplectic quantum mechanics, *International Journal of Modern Physics A*

- 39**, 2450011 (2024).
- [14] C. Dartora, F. Zanella, and G. Cabrera, Emergence of fractional quantum mechanics in condensed matter physics, *Physics Letters A* **415**, 127643 (2021).
- [15] B. A. Stickler, Potential condensed-matter realization of space-fractional quantum mechanics: The one-dimensional Lévy crystal, *Phys. Rev. E* **88**, 012120 (2013).
- [16] P. Chatterjee and R. Modak, One-dimensional lévy quasicrystal, *Journal of Physics: Condensed Matter* **35**, 505602 (2023).
- [17] C. Dartora, The breaking of Mermin-Wagner-Hohenberg's theorem for fractional systems, *Physics Letters A* **496**, 129318 (2024).
- [18] B. Roy and V. Juričić, Correlated fractional dirac materials, *Phys. Rev. Res.* **5**, L032002 (2023).
- [19] J. P. Provost and G. Vallee, Riemannian structure on manifolds of quantum states, *Communications in Mathematical Physics* **76**, 289 (1980).
- [20] R. Resta, M. Posternak, and A. Baldereschi, Towards a quantum theory of polarization in ferroelectrics: The case of knb_3 , *Phys. Rev. Lett.* **70**, 1010 (1993).
- [21] D. Vanderbilt and R. D. King-Smith, Electric polarization as a bulk quantity and its relation to surface charge, *Phys. Rev. B* **48**, 4442 (1993).
- [22] D. Ceresoli, T. Thonhauser, D. Vanderbilt, and R. Resta, Orbital magnetization in crystalline solids: Multi-band insulators, chern insulators, and metals, *Phys. Rev. B* **74**, 024408 (2006).
- [23] R. Resta, The insulating state of matter: a geometrical theory, *Eur. Phys. J. B* **79**, 121 (2011).
- [24] P. Törmä, Essay: Where can quantum geometry lead us?, *Phys. Rev. Lett.* **131**, 240001 (2023).
- [25] X. Hu, T. Hyart, D. I. Pikulin, and E. Rossi, Geometric and conventional contribution to the superfluid weight in twisted bilayer graphene, *Phys. Rev. Lett.* **123**, 237002 (2019).
- [26] Tian, Haidong and Gao, Xueshi, and Zhang, Yuxin and Che, Shi and Xu, Tianyi and Cheung, Patrick and Watanabe, Kenji and Taniguchi, Takashi and Randeria, Mohit and Zhang, Fan and Lau, Chun Ning and Bockrath, Marc W., Evidence for dirac flat band superconductivity enabled by quantum geometry, *Nature* **614**, 440 (2023).
- [27] A. Julku, T. J. Peltonen, L. Liang, T. T. Heikkilä, and P. Törmä, Superfluid weight and Berezinskii-Kosterlitz-Thouless transition temperature of twisted bilayer graphene, *Phys. Rev. B* **101**, 060505 (2020).
- [28] T. Kitamura, S. Kanasugi, M. Chazono, and Y. Yanase, Quantum geometry induced anapole superconductivity, *Phys. Rev. B* **107**, 214513 (2023).
- [29] T. Kitamura, A. Daido, and Y. Yanase, Spin-triplet superconductivity from quantum-geometry-induced ferromagnetic fluctuation, *Phys. Rev. Lett.* **132**, 036001 (2024).
- [30] A. Daido, T. Kitamura, and Y. Yanase, Quantum geometry encoded to pair potentials, *Phys. Rev. B* **110**, 094505 (2024).
- [31] K. H. A. Villegas and B. Yang, Anomalous Higgs oscillations mediated by Berry curvature and quantum metric, *Phys. Rev. B* **104**, L180502 (2021).
- [32] K. H. A. Villegas, Theory of pseudospin resonance for multiband superconductors, *Phys. Rev. B* **108**, 174504 (2023).
- [33] J. Yu, C. J. Ciccarino, R. Bianco, I. Errea, P. Narang, and B. A. Bernevig, Non-trivial quantum geometry and the strength of electron-phonon coupling, *Nature Physics* **20**, 1262 (2024).
- [34] A. B. Bernevig and T. L. Hughes, in *Topological insulators and topological superconductors* (Princeton University Press, 2013).
- [35] D. Vanderbilt, in *Berry Phases in Electronic Structure Theory* (Cambridge University Press, 2018).
- [36] T. Thonhauser, D. Ceresoli, D. Vanderbilt, and R. Resta, Orbital magnetization in periodic insulators, *Phys. Rev. Lett.* **95**, 137205 (2005).
- [37] T. Thonhauser, Theory of orbital magnetization in solids, *International Journal of Modern Physics B* **25**, 1429 (2011), <https://doi.org/10.1142/S0217979211058912>.
- [38] S. Grover, M. Bocarsly, A. Uri, P. Stepanov, G. Di Battista, I. Roy, J. Xiao, A. Y. Meltzer, Y. Myasoedov, K. Pareek, K. Watanabe, T. Taniguchi, B. Yan, A. Stern, E. Berg, D. K. Efetov, and E. Zeldov, Chern mosaic and berry-curvature magnetism in magic-angle graphene, *Nature Physics* **18**, 885 (2022).
- [39] D. Xiao, W. Yao, and Q. Niu, Valley-contrasting physics in graphene: Magnetic moment and topological transport, *Phys. Rev. Lett.* **99**, 236809 (2007).
- [40] G. Jiang, P. Törmä, and Y. Barlas, Superfluid weight crossover and critical temperature enhancement in singular flat bands (2024), arXiv:2407.14919 [cond-mat.suprcon].
- [41] D. D. Solnyshkov, C. Leblanc, L. Bessonart, A. Nalitov, J. Ren, Q. Liao, F. Li, and G. Malpuech, Quantum metric and wave packets at exceptional points in non-hermitian systems, *Phys. Rev. B* **103**, 125302 (2021).
- [42] Q. Liao, C. Leblanc, J. Ren, F. Li, Y. Li, D. Solnyshkov, G. Malpuech, J. Yao, and H. Fu, Experimental measurement of the divergent quantum metric of an exceptional point, *Phys. Rev. Lett.* **127**, 107402 (2021).